nature chemistry

ARTICLES

PUBLISHED ONLINE: 19 FEBRUARY 2012 | DOI: 10.1038/NCHEM.1269

Chemically homogeneous and thermally reversible oxidation of epitaxial graphene

Md. Zakir Hossain[1†], James E. Johns[1,2], Kirk H. Bevan[3†], Hunter J. Karmel[1], Yu Teng Liang[1], Shinya Yoshimoto[4], Kozo Mukai[4], Tatanori Koitaya[4], Jun Yoshinobu[4], Maki Kawai[5,6], Amanda M. Lear[7], Larry L. Kesmodel[8], Steven L. Tait[7] and Mark C. Hersam[1,2,9]*

With its exceptional charge mobility, graphene holds great promise for applications in next-generation electronics. In an effort to tailor its properties and interfacial characteristics, the chemical functionalization of graphene is being actively pursued. The oxidation of graphene via the Hummers method is most widely used in current studies, although the chemical inhomogeneity and irreversibility of the resulting graphene oxide compromises its use in high-performance devices. Here, we present an alternative approach for oxidizing epitaxial graphene using atomic oxygen in ultrahigh vacuum. Atomic-resolution characterization with scanning tunnelling microscopy is quantitatively compared to density functional theory, showing that ultrahigh-vacuum oxidization results in uniform epoxy functionalization. Furthermore, this oxidation is shown to be fully reversible at temperatures as low as 260 °C using scanning tunnelling microscopy and spectroscopic techniques. In this manner, ultrahigh-vacuum oxidation overcomes the limitations of Hummers-method graphene oxide, thus creating new opportunities for the study and application of chemically functionalized graphene.

Graphene is an atomically thin honeycomb lattice of carbon that is the two-dimensional analogue of the polymer polyacetylene. Although its extraordinary electrical mobility[1] and mechanical properties[2] have inspired initial attempts to use graphene in simple circuits including radiofrequency mixers[3], it is unlikely that graphene alone will fulfill the needs of modern-day complex electronic systems. Drawing inspiration from the chemical modification of polyacetylene[4], which enables substantial tunability in its electrical conductivity and has spawned a myriad of organic electronic, optoelectronic and photovoltaic devices, the research community is actively exploring methods for covalently[5–9] and non-covalently[10–12] functionalizing graphene.

Known for over 150 years[13], oxidized graphite, which can be exfoliated into two-dimensional graphene oxide, is the most studied chemically modified form of graphene[14]. Graphene oxide is most commonly synthesized using an aggressive acidic treatment developed by Hummers and Offeman[15], resulting in a chemically inhomogeneous surface with a range of oxygen functional groups and structural defects that degrade the charge mobility by several orders of magnitude[16]. Based on extensive nuclear magnetic resonance, infrared absorption and electron diffraction studies, it has been shown that carboxylic, hydroxyl and carbonyl groups are present at the edge of the graphene oxide sheet, and the basal plane is covered with epoxy and hydroxyl groups[16]. Although chemical[17] or thermal[18] reduction of Hummers-method graphene oxide partially recovers the structure and electrical properties of pristine graphene, the oxygen content of the reduced graphene oxide remains at ~8–10%, and nearly 20% of the carbon retains an sp^3 character[18–20]. Consequently, although graphene oxide is a promising component of paper-like materials[21] and polymer composites[22], reduced graphene oxide has inferior electrical properties when compared to pristine graphene[18–20], thus limiting its ultimate utility in high-performance electronics.

Here, we demonstrate that atomic oxygen prepared in ultrahigh-vacuum (UHV) conditions overcomes the limitations of Hummers-method graphene oxide, resulting in chemically homogeneous and fully reversible oxidization of epitaxial graphene on SiC(0001). The structure of UHV oxidized epitaxial graphene was studied at the atomic scale using scanning tunnelling microscopy (STM) and density functional theory (DFT) and strongly suggests uniform epoxy functionalization. Furthermore, thermal reversibility at temperatures as low as 260 °C was verified with STM, high-resolution core-level X-ray photoelectron spectroscopy (XPS), Raman spectroscopy and ultraviolet photoelectron spectroscopy (UPS), which implies compatibility with technologies that require low-temperature processing. The chemisorbed oxygen can also be reversibly desorbed with STM electrons, thus enabling nanopatterning of covalently modified graphene at the atomic scale. Overall, UHV oxidized graphene presents new opportunities for studying and manipulating the chemistry of graphene in addition to providing a promising two-dimensional nanomaterial platform for a range of applications including integrated circuits, optical communications and photovoltaic technologies.

Results and discussion

UHV oxidation of epitaxial graphene. UHV-based oxidation and reduction is demonstrated here with epitaxial graphene on SiC(0001). Atomic oxygen is produced by cracking O_2 molecules

[1]Department of Materials Science and Engineering, Northwestern University, Evanston, Illinois 60208, USA, [2]Department of Medicine, Northwestern University, Evanston, Illinois 60208, USA, [3]Materials Science and Technology Division, Oak Ridge National Laboratory, Oak Ridge, Tennessee 37831, USA, [4]The Institute for Solid State Physics, University of Tokyo, Kashiwa, Chiba, Japan, [5]Department of Advanced Materials Science, University of Tokyo, Kashiwa, Chiba, Japan, [6]Advanced Science Institute, RIKEN, Wako, Japan, [7]Department of Chemistry, Indiana University, Bloomington, Indiana 47405, USA, [8]Department of Physics, Indiana University, Bloomington, Indiana 47405, USA, [9]Department of Chemistry, Northwestern University, Evanston, Illinois 60208, USA; †Present address: Advanced Engineering Research Team, Advanced Scientific Research Leaders Development Unit, Gunma University, Kiryu-City 376-8515, Japan (M.Z.H.), Department of Mining and Materials Engineering, McGill University, Montreal, Quebec H3A 2T8, Canada (K.H.B.). *e-mail: m-hersam@northwestern.edu

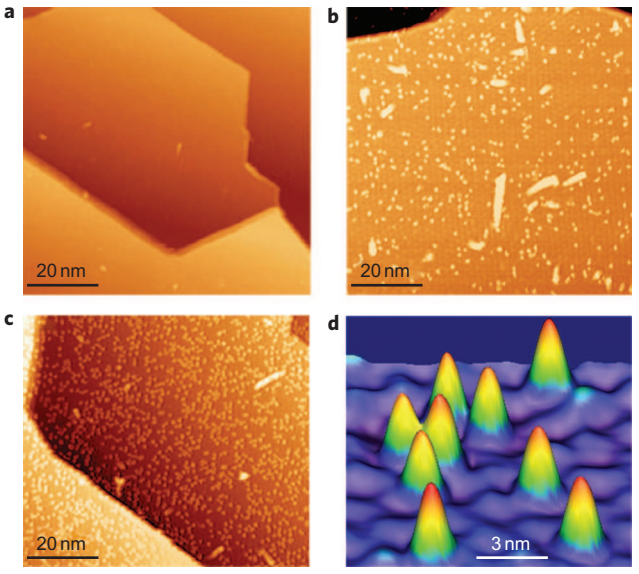

Figure 1 | Atomic-scale imaging of chemisorbed atomic oxygen on epitaxial graphene. a–c, STM image of epitaxial graphene as-prepared (**a**) and following exposure to 600 L (**b**) and 2,400 L (**c**) of atomic oxygen. Bright protrusions randomly distributed over the surface are attributed to chemisorbed oxygen species, while the irregularly shaped one-dimensional features are common defects on epitaxial graphene that are independent of the oxidation treatment. **d**, High-resolution, three-dimensionally rendered STM image of nine chemisorbed oxygen atoms on epitaxial graphene. All STM images were acquired at a sample bias of +2.4 V and a tunnelling current of 50 pA.

on a hot (~1,500 °C) tungsten filament under UHV conditions. The atomic oxygen chemisorbs to the basal plane of epitaxial graphene and appears as bright protrusions in STM images. Figure 1 presents STM images of epitaxial graphene before (Fig. 1a) and after (Fig. 1b) exposure to atomic oxygen. The presence of oxygen on the surface was verified with Auger electron spectroscopy (AES) (Supplementary Section S1). The bright protrusions randomly distributed across the surface are attributed to chemisorbed oxygen. By controlling the duration of atomic oxygen exposure, the level of epitaxial graphene oxidation can be readily tuned, as shown in Fig. 1b,c. In this regime (<0.01 ML (monolayer)), the coverage of chemisorbed oxygen increases linearly with dose of atomic oxygen. Although epitaxial graphene on SiC(0001) has regions of both single and bilayer graphene, no significant differences in the concentration of chemisorbed oxygen are observed as a function of epitaxial graphene thickness. The one-dimensional features observed in Fig. 1a–c are common defects for epitaxial graphene that are unrelated to and have no observable effect on the UHV oxidation process.

Although the chemisorbed oxygen is stable under typical imaging conditions at positive sample bias, tip-induced desorption readily occurs at negative bias. This desorption therefore precludes STM imaging at negative sample biases, but it does suggest the reversibility of epitaxial graphene oxidation and presents opportunities for nanoscale patterning, as will be discussed in more detail in the following. Careful inspection reveals that each oxygen feature has a uniform appearance in STM images (Fig. 1d), which suggests a chemically uniform binding state for atomic oxygen on epitaxial graphene.

The lateral diameter of the oxygen features observed in the STM images is ~1.2 nm (Fig. 2a), which is approximately eight times greater than the C–C bond length of graphene. As this relatively large size is measured even when atomic resolution is observed on the surrounding graphene lattice, we conclude that it cannot be explained by an imaging artefact related to the finite size of the STM tip. Oxygen clustering is also an unlikely explanation, because increasing the oxygen dose leads to the appearance of additional identically sized features rather than increasing the size of pre-existing features, even in the limit of low coverage. Other possible explanations include a relatively long-range perturbation of the surface electronic structure around the chemisorbed oxygen and/or a geometrical distortion of the underlying epitaxial graphene due to strain release upon chemisorption[23,24].

DFT. In an effort to develop a quantitative understanding of the STM images, we performed DFT calculations within the local density approximation (LDA). Epitaxial graphene thermally grown on top of SiC(0001) is compressively strained because the graphene expands and the SiC contracts during cooling[23,24]. This compressive strain is not entirely released through graphene buckling or warping, due to a critical compressive strain release barrier arising from π–π orbital interactions within the graphene lattice[25]. For uniaxial compression, *ab initio* calculations place this critical compression value at –1.25% (ref. 25). Our DFT calculations suggest that the presence (or absence) of compressive strain has a pronounced effect on the apparent lateral size of oxygen adatoms. Without strain, the simulated oxygen epoxy structure, which is the lowest energy adsorption state of oxygen adatoms on graphene[26], results in a subtle topographic protrusion with a lateral diameter of ~0.5 nm. However, at the maximum graphene/SiC compressive strain value of –0.8% (ref. 23), the simulated topography of an isolated epoxy structure increases markedly, leading to a lateral diameter of ~1.3 nm (Fig. 2b). We therefore suggest that oxygen adatoms on epitaxial graphene perturb the planar π–π interactions of the graphene lattice through sp^3 bonding, and thereby act as strain release centres that allowing buckling to occur. In other words, oxygen chemisorption induces topographic distortion of epitaxial graphene in the region

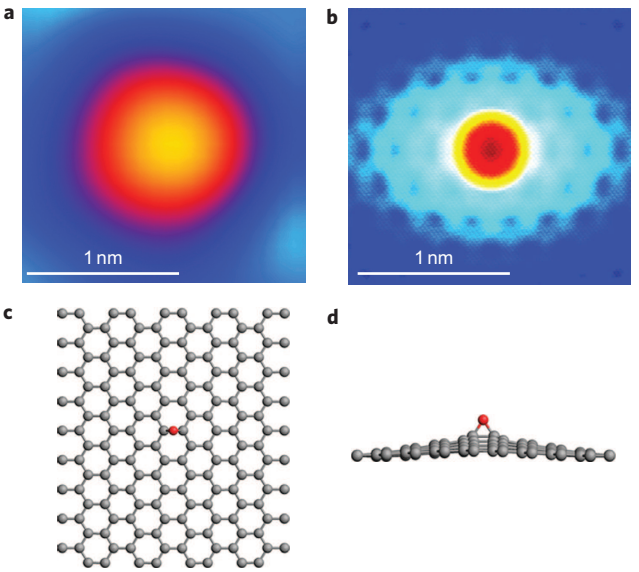

Figure 2 | Comparison of STM images and DFT calculations of oxygen adatoms on epitaxial graphene. a,b, Experimental (**a**) and simulated (**b**) STM images of an isolated chemisorbed oxygen epoxy structure on epitaxial graphene. The STM image was acquired at a sample bias of +2.4 V and a tunnelling current of 50 pA. The simulated STM images were generated within the Tersoff-Hamman approximation. **c,d**, Top (**c**) and side (**d**) views of the lowest energy configuration of oxygen adatoms on –0.8% strained graphene.

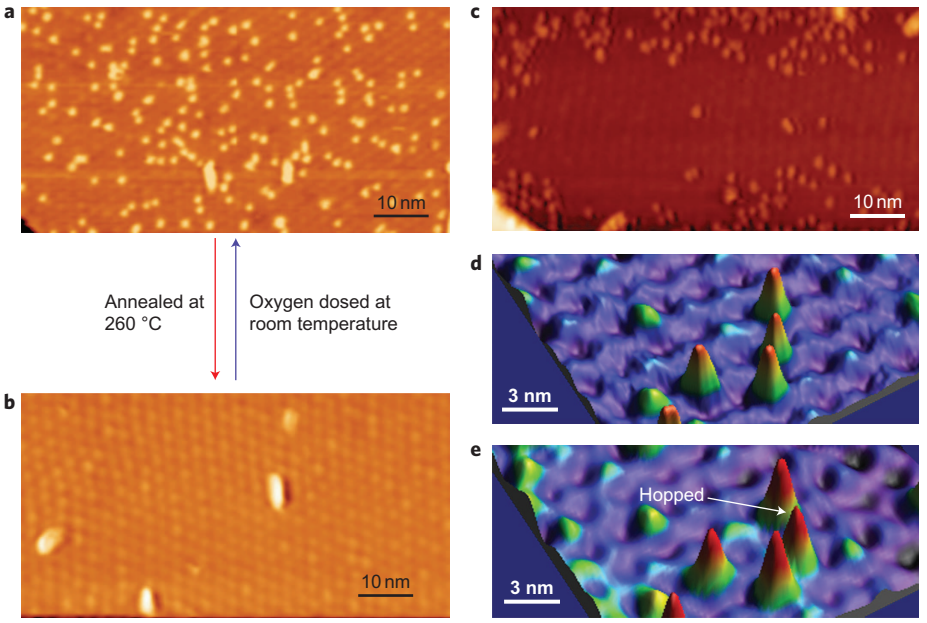

Figure 3 | Reversible UHV oxidation and reduction of epitaxial graphene. a,b, STM images of UHV oxidized epitaxial graphene before (**a**) and after (**b**) annealing at 260 °C. **c**, STM image showing a region of the UHV oxidized epitaxial graphene surface where chemisorbed oxygen has been reversibly desorbed by injecting electrons from the STM tip at a sample bias of +4.0 V and tunnelling current of 1 nA. **d,e**, STM images before (**d**) and after (**e**) hopping of chemisorbed oxygen on epitaxial graphene at room temperature. The displaced oxygen adatom is indicated in **e**. All STM images were acquired at a sample bias of +2.4 V and a tunnelling current of 50 pA.

surrounding the oxygen bonding site (Fig. 2c,d), resulting in the relatively large feature observed with STM (Fig. 2a).

Desorption of chemisorbed oxygen. Although the chemisorbed oxygen is stable at room temperature and under normal STM imaging conditions, it can be reversibly removed by annealing the oxidized surface at 260 °C or scanning the surface at elevated sample bias and/or tunnelling current. Figure 3a,b show STM images of an oxidized graphene surface before and after annealing the surface at 260 °C, respectively. The surface observed in Fig. 3b appears identical to the initial epitaxial graphene surface, with no evidence of the previously chemisorbed oxygen. Furthermore, when the reduced surface shown in Fig. 3b is again exposed to atomic oxygen, an oxidized surface comparable to that of Fig. 3a is reestablished. These results suggest that the original pristine epitaxial graphene surface can be recovered by thermal reduction of the oxidized surface; that is, the UHV oxidation–reduction process is fully reversible, in stark contrast to the highly defective and partially oxidized surface that results from the reduction of Hummers-method graphene oxide[19,20].

Chemisorbed oxygen on epitaxial graphene can also be reversibly desorbed with energetic electrons from the STM tip. Figure 3c presents an STM image following exposure of a region of the oxidized epitaxial graphene surface to elevated tunnelling conditions (sample bias, 4.0 V; tunnelling current, 1 nA). The clean area observed in the STM image (Fig. 3c) indicates STM tip-induced desorption of chemisorbed oxygen. Furthermore, the integrity of the graphene mesh following desorption of chemisorbed oxygen is confirmed by atomic-resolution STM imaging (Supplementary Section S2). The relatively modest tunnelling conditions for STM-induced desorption suggest a clear pathway for atomically precise nanopatterning on oxidized epitaxial graphene with established nanolithography techniques such as feedback-controlled lithography[27]. Lateral displacement of individual oxygen atoms is also observed at room temperature (Fig. 3d,e). The low electronic and thermal energies required to desorb or displace oxygen suggest that the binding energy is relatively low, which is consistent with the epoxy bond assignment[26].

Spectroscopic verification. To verify the identity of chemisorbed species and the reversibility of the UHV oxidation–reduction process of epitaxial graphene, high-resolution core-level XPS (HR-XPS), Raman spectroscopy and UPS measurements were performed (Fig. 4). Figure 4a shows an STM image of oxidized epitaxial graphene at the surface coverage used for this spectroscopic characterization. Because XPS is widely used for characterization of the chemical bonding state of oxidized carbonaceous materials including highly ordered pyrolytic graphite[17,28,29], HR-XPS was performed on UHV-oxidized epitaxial graphene. In the HR-XPS spectrum of Fig. 4b (red curve), the C1*s* peak at 286.3 eV, which is located at 1.8 eV higher binding energy than the sp^2 C1*s* peak of graphene, is ascribed to the epoxy species on the oxidized epitaxial graphene surface[28–30]. Additional details concerning the C1*s* and O1*s* spectrum, including the graphene and substrate SiC peaks, can be found in Supplementary Figs S3 and S4. Following annealing at 260 °C, the C1*s* peak corresponding to the epoxy species completely disappears, and the spectrum of pristine epitaxial graphene is reestablished (Fig. 4b, blue curve).

The Raman spectra of oxidized epitaxial graphene before and after annealing at 260 °C are presented in Fig. 4c. The main features in these Raman spectra are the D and 2D peaks that lie at ~1,360 and 2,755 cm^{-1}, respectively[24,26]. The G band overlaps with SiC substrate-induced Raman peaks, which complicates its interpretation[24]. The D peak is optically inactive in pristine graphene monolayers, and is generally attributed to disorder and sp^3 bonding in the graphene lattice. The presence of a small D peak even on pristine epitaxial graphene arises from strong coupling to the underlying SiC substrate. The 2D band is optically allowed in graphene, and the ratio of the D and 2D peaks can be used as a measure of disorder when the G peak is obscured. In Fig. 4c, the D/2D intensity ratio is relatively high for oxidized epitaxial graphene (red curve) and then reduces to the value of pristine epitaxial graphene following annealing at 260 °C (blue curve). A similar reversibility is observed in the

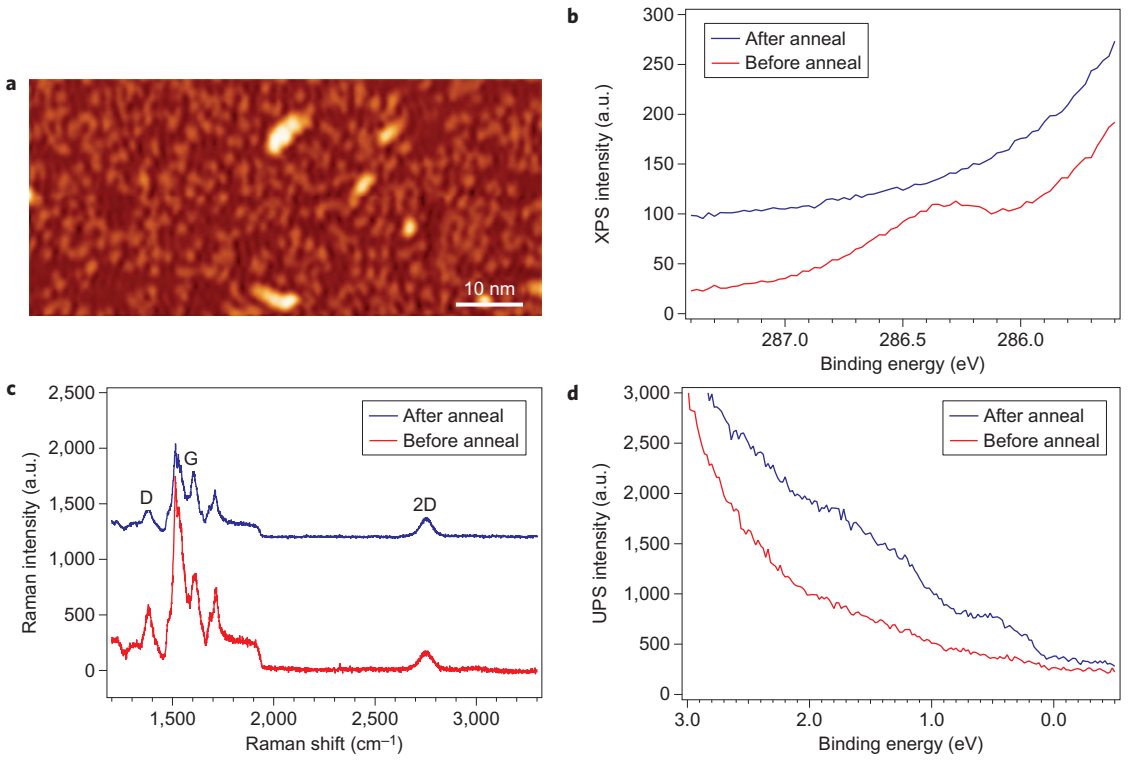

Figure 4 | Spectroscopic verification of the reversibility of UHV oxidized epitaxial graphene. a, STM image of oxidized epitaxial graphene at the surface coverage used for subsequent spectroscopic characterization (sample bias, +2.4 V; tunnelling current, 50 pA). **b**, C1s HR-XPS acquired at a photon energy of 403 eV of oxidized epitaxial graphene before and after annealing at 260 °C (spectra offset vertically for clarity). The peak at 286.3 eV indicative of epoxy species disappears following annealing. **c**, Raman spectroscopy of oxidized epitaxial graphene before and after annealing at 260 °C. The Raman spectra are normalized to the 2D peak intensity and offset vertically for clarity. The D/2D intensity ratio reduces to the value observed for pristine epitaxial graphene following annealing. **d**, UPS of oxidized epitaxial graphene before and after annealing at 260 °C. The UPS intensity increases to the values observed for pristine epitaxial graphene following annealing.

Raman spectra of chemical vapour deposition (CVD) graphene on copper foil, as shown in Supplementary Fig. S5.

Figure 4d shows the UPS spectra of oxidized epitaxial graphene before and after annealing at 260 °C. The UPS spectrum of the oxidized epitaxial graphene surface is nearly featureless (red curve), which implies a low electronic density of states, as would be expected for oxidized graphene. In contrast, after annealing at 260 °C, the electronic density of states increases at binding energies of ~0.5 and 1.5 eV (blue curve). The UPS spectrum following annealing agrees well with previous observations for pristine epitaxial graphene[31]. Overall, the UPS results suggest that the electronic density of states in the low binding energy region, which can be attributed to the π-states of the graphene surface[5], is attenuated upon chemisorption of oxygen and regenerated following annealing at 260 °C.

Conclusions

In summary, atomic oxygen exposure under UHV conditions leads to a chemically homogeneous and reversible covalent modification of epitaxial graphene. STM reveals that atomic oxygen chemisorbs in a highly uniform manner to the basal plane of epitaxial graphene, resulting in the appearance of ~1.2-nm-diameter protrusions that agree well with DFT calculations of isolated epoxy groups on a strained epitaxial graphene/SiC substrate. The oxidation is reversible, as STM, HR-XPS, Raman spectroscopy and UPS verify that thermal annealing at 260 °C in UHV fully reduces the surface back to pristine epitaxial graphene. In addition, oxygen desorption or lateral displacement can be locally induced with energetic electrons from the STM tip, thus providing a pathway to atomically precise nanopatterning of the oxidized epitaxial graphene surface. The demonstration of a chemically homogeneous and reversible oxidation of graphene overcomes the limitations of Hummers-method graphene oxide, and represents an important step towards realizing new classes of two-dimensional nanomaterials by chemical modification of graphene.

Methods

Preparation and UHV STM characterization of oxidized epitaxial graphene. Epitaxial graphene was prepared by annealing n-type 6H-SiC(0001) samples (Cree, Inc.) at 1,350 °C for 10–12 cycles of 30 s under UHV conditions (maximum pressure, $\sim 5.0 \times 10^{-9}$ torr). STM imaging of the silicon face of the epitaxial graphene/SiC substrate was accomplished at room temperature using a homebuilt UHV STM (pressure, $\sim 5.0 \times 10^{-11}$ torr)[32]. UHV oxidation was carried out by cracking O_2 into atomic oxygen on a hot (~1,500 °C) tungsten filament located ~7 cm away from the epitaxial graphene sample. During oxidation, the temperature of the epitaxial graphene sample was maintained below 0 °C with an O_2 pressure of $\sim 2.0 \times 10^{-6}$ torr. The total O_2 dose is expressed in Langmuirs ($1\ L = 1.0 \times 10^{-6}$ torr s).

DFT calculations. Using a double-ζ polarized basis and a real space grid of 4,082 eV, the graphene 9 × 9 structures were relaxed through the conjugate gradient method to a force tolerance of 0.01 eV $Å^{-1}$ (ref. 33). Lateral periodic interactions were captured at 4 × 4 *k*-points for relaxations and 12 × 12 *k*-points for STM image simulations, with an in-plane vacuum region of 17 Å. For the local density of states simulated image (Fig. 2b), the substrate Fermi level was situated 0.4 eV above the graphene Dirac point[31].

HR-XPS. HR-XPS measurements were performed using a Scienta SES-200 at the Photon Factory BL13A (KEK-PF PAC 2009-S2-007), Japan. The incident and emission angles with respect to the surface normal for the photon and photoelectron beams were 65° and 0°, respectively. The total energy resolution was ~70 meV. The electron binding energy was referenced to the C1*s* peak of bulk SiC at 283.73 eV (ref. 34).

Raman spectroscopy. Raman measurements were carried out using <5 mW of 514.5 nm light from an argon/krypton laser in a confocal geometry with a 0.85 NA,

×100 objective. The beam spot size was 2–3 μm. Spectra were taken using a single stage of a Princeton Instruments Trivista 777 spectrograph with a 1,800 grooves/mm grating and a LN_2 cooled charge-coupled device. The Raman shift axis was scaled to reproduce the known shifts of cyclohexane and silicon. The exposure for each spectrum was less than 5 min, and no evidence of laser-induced damage was observed.

UPS. UPS spectra were gathered at room temperature using an Omicron EA 125 electron spectrometer at a photon energy of 21.2 eV (He I) under UHV conditions (pressure, $\sim 5.0 \times 10^{-11}$ torr). The diameter of the ultraviolet light irradiation was ~1.5 mm. The incident and emission angles with respect to the surface normal for the ultraviolet light and photoelectron were 45° and 0°, respectively.

Received 17 November 2011; accepted 13 January 2012; published online 19 February 2012

References

1. Morozov, S. V. *et al.* Giant intrinsic carrier mobilities in graphene and its bilayer. *Phys. Rev. Lett.* **100,** 016602 (2008).
2. Lee, C., Wei, X., Kysar, J. W. & Hone, J. Measurement of the elastic properties and intrinsic strength of monolayer graphene. *Science* **321,** 385–388 (2008).
3. Lin, Y. -M. *et al.* Wafer-scale graphene integrated circuit. *Science* **332,** 1294–1297 (2011).
4. Chiang, C. K. *et al.* Synthesis of highly conducting films of derivatives of polyacetylene. *J. Am. Chem. Soc.* **100,** 1013–1015 (1978).
5. Elias, D. C. *et al.* Control of graphene's properties by reversible hydrogenation: evidence for graphane. *Science* **323,** 610–613 (2009).
6. Robinson, J. T. *et al.* Properties of fluorinated graphene films. *Nano Lett.* **10,** 3001–3005 (2010).
7. Nair, R. R. *et al.* Fluorographene: a two-dimensional counterpart of Teflon. *Small* **6,** 2877–2884 (2010).
8. Niyogi, S. *et al.* Spectroscopy of covalently functionalized graphene. *Nano Lett.* **10,** 4061–4066 (2010).
9. Hossain, M. Z., Walsh, M. A. & Hersam, M. C. Scanning tunneling microscopy, spectroscopy, and nanolithography of epitaxial graphene chemically modified with aryl moieties. *J. Am. Chem. Soc.* **132,** 15399–15403 (2010).
10. Chen, W., Chen, S., Qi, D. C., Gao, X. Y. & Wee, A. T .S. Surface transfer p-type doping of epitaxial graphene. *J. Am. Chem. Soc.* **129,** 10418–10422 (2007).
11. Wang, X., Tabakman, S. M. & Dai, H. Atomic layer deposition of metal oxides on pristine and functionalized graphene. *J. Am. Chem. Soc.* **130,** 8152–8153 (2008).
12. Wang, Q. H. & Hersam, M. C. Room-temperature molecular-resolution characterization of self-assembled organic monolayers on epitaxial graphene. *Nature Chem.* **1,** 206–211 (2009).
13. Brodie, B. C. On the atomic weight of graphite. *Phil. Trans. R. Soc.* **149,** 249–259 (1859).
14. Park, S. & Ruoff, R. S. Chemical methods for the production of graphenes. *Nature Nanotech.* **4,** 317–224 (2009).
15. Hummers, W. S. & Offeman, R. E. Preparation of graphitic oxide. *J. Am. Chem. Soc.* **80,** 1339 (1958).
16. Dreyer, D. R., Park, S., Bielawski, C. W. & Ruoff, R. S. The chemistry of graphene oxide. *Chem. Soc. Rev.* **39,** 228–240 (2010).
17. Stankovich, S. *et al.* Synthesis of graphene-based nanosheets via chemical reduction of exfoliated graphene oxide. *Carbon* **45,** 1558–1565 (2007).
18. Becerril, H. A., Mao, J., Liu, Z., Stoltenberg, R. M., Bao, Z. & Chen, Y. Evaluation of solution-processed reduced graphene oxide films as transparent conductors. *ACS Nano* **2,** 463–470 (2008).
19. Gomez-Navarro, C. *et al.* Atomic structure of reduced graphene oxide. *Nano Lett.* **10,** 1144–1148 (2010).
20. Bagri, A. *et al.* Structural evolution during the reduction of chemically derived graphene oxide. *Nature Chem.* **2,** 581–587 (2010).
21. Dikin, D. A. *et al.* Preparation and characterization of graphene oxide paper. *Nature* **448,** 457–460 (2007).
22. Park, S. *et al.* Biocompatible, robust free-standing paper composed of a TWEEN/graphene composite. *Adv. Mater.* **22,** 1736–1740 (2010).
23. Ferralis, N., Maboudian, R. & Carraro, C. Evidence of structural strain in epitaxial graphene layers on 6H-SiC(0001). *Phys. Rev. Lett.* **101,** 156801 (2008).
24. Röhrl, J. *et al.* Raman spectra of epitaxial graphene on SiC(0001). *Appl. Phys. Lett.* **92,** 201918 (2008).
25. Kumar, S., Hembram, K. P. & Waghmare, U. V. Intrinsic buckling strength of graphene: first-principles density functional theory calculations. *Phys. Rev. B* **82,** 115411 (2010).
26. Kudin, K. N. *et al.* Raman spectra of graphite oxide and functionalized graphene sheets. *Nano Lett.* **8,** 36–39 (2008).
27. Wang, Q. H. & Hersam, M. C. Nanofabrication of heteromolecular organic nanostructures on epitaxial graphene via room temperature feedback-controlled lithography. *Nano Lett.* **11,** 589–593 (2011).
28. Barinov, A. *et al.* Initial stages of oxidation on graphitic surfaces: photoemission study and density functional theory calculations. *J. Phys. Chem. C* **113,** 9009–9013 (2009).
29. Vinogradov, N. A. *et al.* Impact of atomic oxygen on the structure of graphene formed on Ir(111) and Pt(111). *J. Phys. Chem. C* **115,** 9568–9577 (2011).
30. Larciprete, R. *et al.* Dual path mechanism in the thermal reduction of graphene oxide. *J. Am. Chem. Soc.* **133,** 17315–17321 (2011).
31. Coletti, C. *et al.* Charge neutrality and band-gap tuning of epitaxial graphene on SiC by molecular doping. *Phys. Rev. B* **81,** 235401 (2010).
32. Foley, E. T., Yoder, N. L., Guisinger, N. P. & Hersam, M. C. Cryogenic variable temperature ultra-high vacuum scanning tunneling microscope for single molecule studies on silicon surfaces. *Rev. Sci. Instrum.* **75,** 5280–5287 (2004).
33. Soler, J. M. *et al.* The SIESTA method for *ab initio* order-*N* materials simulation. *J. Phys. Condens. Matter* **14,** 2745–2779 (2002).
34. Riedl, C., Coletti, C. & Starke, U. Structural and electronic properties of epitaxial graphene on SiC(0001): a review of growth, characterization, transfer doping and hydrogen intercalation. *J. Phys. D* **43,** 374009 (2010).

Acknowledgements

This work was supported by the National Science Foundation (award nos EEC-0647560, DMR-0906025 and DMR-1121262), the Office of Naval Research (award nos N00014-09-1-0180 and N00014-11-1-0463) and the US Department of Energy (award no. DE-SC0001785). K.H.B. acknowledges support from NSERC (Canada), M.C.H. acknowledges a W. M. Keck Foundation Science and Engineering Grant, and M.Z.H. acknowledges partial support by the Program to Disseminate Tenure-Track System of the Ministry of Education, Culture, Sports, Science and Technology of Japan (MEXT) granted to Gunma University. The authors thank J. Lyding for the use of his STM control software. S.Y., K.M., T.K. and J.Y. thank K. Mase at KEK-PF for maintenance of BL13A. Computational resources were provided by the National Science Foundation Network for Computational Nanotechnology.

Author contributions

M.Z.H. developed the UHV oxidation procedures for epitaxial graphene, performed STM, XPS and UPS characterization and analysis, and wrote the first draft of the manuscript. J.E.J. and Y.T.L. performed the Raman spectroscopy and analysis. K.H.B. performed the DFT calculations and analysis. H.J.K. contributed to the experimental set-up for dosing oxygen in UHV. A.M.L., S.L.T. and L.L.K. performed AES characterization and analysis. S.Y., K.M., T.K. and J.Y. performed the HR-XPS measurements. M.K. contributed to the UPS measurement. M.C.H. oversaw all research phases and revised the manuscript in collaboration with all co-authors.

Additional information

The authors declare no competing financial interests. Supplementary information accompanies this paper at www.nature.com/naturechemistry. Reprints and permission information is available online at http://www.nature.com/reprints. Correspondence and requests for materials should be addressed to M.C.H.